International Journal of Vehicle Design

ISSN online: 1741-5314 - ISSN print: 0143-3369
https://www.inderscience.com/ijvd

Design and evaluation of a driver intent based mobile control interface for ground vehicles

Chengshi Wang, Kim Alexander, Philip Pidgeon, John Wagner

DOI: 10.1504/IJVD.2023.10058871

Article History:

Received:	12 November 2019
Last revised:	03 August 2021
Accepted:	17 September 2021
Published online:	04 September 2023

Design and evaluation of a driver intent based mobile control interface for ground vehicles

Chengshi Wang*

The MathWorks, Inc.,
Natick, MA 01760, USA
Email: chengshw@mathworks.com
*Corresponding author

Kim Alexander and Philip Pidgeon

Institute for Global Road Safety and Security,
Clemson University,
Clemson, SC 29634, USA
Email: kalxndr@clemson.edu

John Wagner

Department of Mechanical Engineering,
Clemson University,
Clemson, SC 29634, USA
Email: jwagner@clemson.edu

Abstract: Drive-by-wire technologies have greatly expanded mobility options for diverse drivers. This study presents a cellphone-inspired portable human-machine-interface (HMI) that integrates directional control, brake, and throttle functionality into a single holistic device. A nonlinear adaptive control technique and an optimal control approach based on driver intent are proposed for combined longitudinal and lateral vehicle guidance. Designed to assist disabled drivers by minimising arm and leg movements, the device was tested in a driving simulator platform. Human subjects evaluated the mechatronic system through obstacle avoidance and city road driving tests, with a conventional steering wheel and pedals used for comparison. Results show that the mobile driving interface with the proposed control scheme improved driver performance by up to 55.8% compared to traditional driving systems during aggressive manoeuvres. The system's superior performance during certain vehicle manoeuvres and participants approval implies its potential as an alternative driving adaptation for disabled drivers.

Keywords: longitudinal and lateral dynamics; vehicle dynamics; nonlinear control; adaptive control; optimal control; state flow control; mobile control interface; portable HMI; emulated cellphone driving device; driver intent; human subject testing; ground vehicles; driver-by-wire.

Reference to this paper should be made as follows: Wang, C., Alexander, K., Pidgeon, P. and Wagner, J. (2023) 'Design and evaluation of a driver intent based mobile control interface for ground vehicles', *Int. J. Vehicle Design*, Vol. 92, No. 1, pp.42–70.

Biographical notes: Chengshi Wang received his BSc degree in Mechanical Engineering from Georgia Institute of Technology, USA, in 2014, and both his MS and PhD degrees in Mechanical Engineering from Clemson University, USA, in 2019 and 2020. His research interests encompass data-based control, haptic interface design in intelligent vehicles, and modeling and control of extensible continuum robots. He previously held a Postdoctoral Appointee position at Argonne National Laboratory, where he conducted research in AI-driven large-scale automated scientific experimental laboratories. He currently serves as a Senior Software Engineer in Test at MathWorks, contributing his expertise in automated driving related products.

Kim Alexander holds BS and MEd degrees with an EdD degree focusing on curriculum development and risk perception training from Clemson University. She is Clemson University's founding Executive Director of the Institute for Global Road Safety and Security (IGRSS). Her primary research interests include attitudinal, cognitive, behavioural, cultural, and social aspects and underlying forces related to road users with the goal of enhancing the safety of the human-vehicle-road environment. She is the Program Director of the Master of Transportation Safety Administration (MTSA) at Clemson University.

Philip Pidgeon holds BA and DMin degrees with an EdD degree focusing on curriculum development and educational leadership from Clemson University. As an educator and researcher, his work investigates the attitudinal, behavioural, cognitive, social, and cultural aspects of road traffic injury prevention, with an eye toward developing effective interventions to enhance the safety of the human-vehicle-road environment. His research experience ranges from studies on the influence of leadership training on road safety education programs to behavioural influence program development for specific subpopulations (including children, young drivers, and military personnel).

John Wagner received the BS, MS, and PhD degrees in Mechanical Engineering from the State University of New York at Buffalo and Purdue University. His research interests include nonlinear control theory, diagnostic/ prognostic methods, digital engineering processes, and mechatronic system design with application to transportation and power generation systems. He is the Director of the PLM Center at Clemson University, and a Fellow of both the ASME and SAE.

This paper is a revised and expanded version of a paper entitled 'Use of cellphones as alternative driver ınputs in passenger vehicles' presented at the *SAE World Congress Experience (WCX) 2019*, Detroit, April 2019.

1 Introduction

The introduction of computer controlled electro-mechanical actuators and human-machine interfaces in automobiles has enhanced autonomous manoeuvres, which fosters superior accessibility, usability, and mobility options for all drivers (Elvin and Gambrell, 2002; Jafari et al., 2016). Recent progress toward drive-by-wire technology has enabled new paradigms in semi-autonomous vehicles (Wang et al., 2018). Steering (Gambrell and Elvin, 2002), braking, and throttle by-wire have laid the groundwork for communication between drivers and computer commanded inputs as well as performance enhancement. Of interest is the combination of these three separate functions into a cellphone-inspired single all-encompassing device: a mobile control HMI. For left and right turns, this portable HMI has steering that rotates clockwise and counterclockwise. Similarly, brake occurs by backward rotation of the mobile control HMI while throttle happens with forward rotation (refer to Figure 1). The value of the driver input signals is represented by the amount of angular rotation in these two angular coordinates. Because drive-by-wire eliminates physical connections between input devices and the vehicle, the driver controls can be placed more flexibly in the cabin within the driver's reach where road visibility permits.

Figure 1 Vehicle control has evolved from a traditional steering wheel with brake and throttle pedals to a mobile control HMI (see online version for colours)

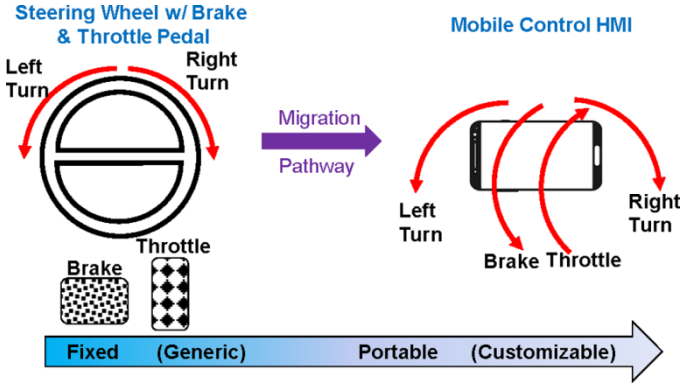

In comparison with traditional driving devices, some of the potential advantages of a portable HMI include more room, driving interface arrangement flexibility, enhanced safety during a car crash by eliminating direct driver contact with steering wheel, and more precise directional control. Furthermore, the mobile control device removes the use of legs during longitudinal manoeuvres by merging the steering mechanism with throttle and brake control, aiding disabled drivers who are unable to manoeuvre their feet onto the gas and brake pedals. In spite of these benefits, the cellphone-inspired driving paradigm also holds several drawbacks such as unintended or accidental control device deflections and wrist fatigue to different extent.

Recent research has investigated how drivers reacted to various steering system and driver input configurations. Fong et al. (2001) developed two novel driving interfaces: GestureDriver which uses visual gesture recognition for operator adaptive vehicle control and HapticDriver which facilitates precision driving via haptic feedback. Matsuura et al. (2004) created a driver's joystick that was tested in-vehicle against a traditional steering

wheel. Shaw et al. (1999) devised a novel steering system that involved the replacement of rigid metal projections into the cabin with flexible plastic ones. Zheng et al. (2017) developed a unique design strategy for joystick system variable yaw rate gain control.The dynamic behaviour of a hydraulic steering system was modelled, simulated, and evaluated by Nahak and Kota (2013). With a fixed-base driving simulator, Andonian et al. (2003) compared the lane trajectory tracking capability of a joystick to that of a steering wheel. Gil et al. (2013) presented a new two degree-of-freedom drive-by-wire mechanism with haptic feedback that couples the steering, accelerating and braking functions. Wang et al. (2019b) investigated three steering interfaces (steering wheel, joystick, and robotic grip) that use haptic feedback to achieve lane keeping functions. The results showed that the robotic arm outperformed the joystick and steering wheel in most cases.

The majority of novel driving interface studies fall into three broad categories: (a) gesturing-based driving interface, (b) joystick-controlled driving interface, and (c) haptic driving interface. However, the literature is short on considering a palm-size HMIs. For some driving applications, installing bulky control devices may be infeasible due to monetary, technical, or environmental constraints. For other applications, the vehicle is driven by a range of operators having diverse backgrounds and for whom extensive training is impractical. The designed portable HMI minimises the need for training and enables rapid command generation to improve situational awareness. Such a driving interface naturally applies to autonomous ground vehicles' teleoperation, which has become the essential and safe enabler of the new mobility in the foreseeable future.

Over the years, extensive control strategies have been proposed to design better and more reliable controllers for the longitudinal and lateral dynamics of ground vehicles. Katriniok et al. (2013) proposed a model-based predictive control approach for combined longitudinal and lateral vehicle guidance. Xu et al. (2016) presents the design of driving control system of both longitudinal and lateral controllers, where several adaptive and robust control algorithms have been integrated for Kuafu-II autonomous vehicle. Guo et al. (2016) constructed a coordinated steering and braking control strategy based on the nonlinear backstepping control theory and the adaptive fuzzy sliding-mode control technique. Attia et al. (2014) proposes a nonlinear model predictive controller for lateral control and a longitudinal control based on a nonlinear control law considering the powertrain dynamics and gearbox ratio. Chebly et al. (2017) covers a coupled control algorithm for longitudinal and lateral dynamics which is realised using Lyapunov functions and is based on the vehicle model that is carried out using the robotics formalism. Guo (2016) designed an adaptive coordinated control scheme to manage longitudinal and lateral motion using adaptive backstepping sliding mode control. For this paper, an integrated lateral and longitudinal control strategy has been adopted based on nonlinear adaptive control theory and optimal preview control technique.

Driver intent prediction is a concept that expresses a decision-making framework and plays a significant role in determining the appropriate state and subsequent course of action when coping with different situations. Past research efforts in driver intent prediction emphasised on the probabilistic method utilising Hidden Markov Models (HMMs) or its special form Bayesian network (Polling et al., 2005; Li et al., 2016). Additional work has been done on driver intent inference used machine learning algorithms that deploy artificial neural network (ANN) models to feed augmented information into a support vector machine (SVM) (Kumar et al., 2013; Kim et al., 2017). To develop an practical driver intention interpretation system for the portable driving

HMI, the rule-based state flow control framework is proposed in this paper. Due to the lower computation complexity and ease of implementation on universal vehicle platforms, the state flow controller switch between different inferred driver intent states triggered by input from the driver and on-board sensors.

Prior study aimed to provide integrated longitudinal and lateral control techniques using brake, throttle, and steering torque to improve vehicle longitudinal and lateral performance. While this paper provides insights on the unified longitudinal and lateral controller, it dedicates a considerable amount of attention to the design and performance evaluation of the portable HMI. In particular, research on alternative driving devices to broaden opportunities for people with disabilities to operate vehicles is notably deficient. The concept of replacing the steering wheel and throttle/brake pedals on ground vehicles is intriguing, and this study aims to fill that gap by examining the novel driving paradigm and comparing its performance to that of the traditional driving system in a driving simulator environment under various road scenarios and speeds.

Figure 2 depicts a high-level diagram of the system. Through quantitative and qualitative measures, this study looked into the possibility of employing a portable HMI as an alternative driver input device in passenger automobiles. The rest of the paper is laid out as follows. Section 2 contains the mathematical theory for nonlinear vehicle dynamics. Section 3 discusses the design of a portable human-vehicle interface. The control algorithms for the unique driving interface are presented in Section 4. Section 5 introduces the experimental methodology, while Section 6 discusses the outcomes of the operator-in-the-loop tests. The conclusion is contained in Section 7.

Figure 2 Closed-loop system design for human/machine driving interface with immersive environment (see online version for colours)

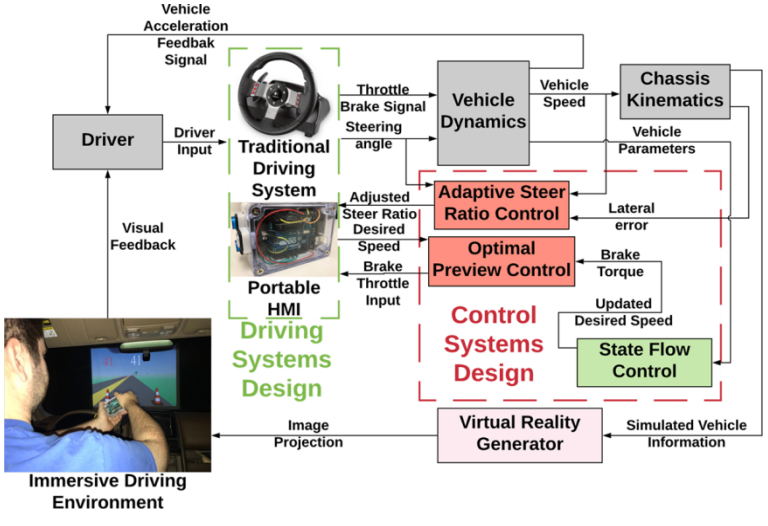

2 Vehicle dynamics model

The longitudinal and lateral vehicle platform characteristics are described by the vehicle dynamics model. The steer-by-wire technology uses a specialised front wheel steering assembly to provide lateral vehicle control.

2.1 Chassis dynamics

The governing equations for the longitudinal velocity, v_x, lateral velocity, v_y, and yaw rate, $\dot{\psi}$, are given by (Freeman et al., 2016)

$$\begin{aligned} m\dot{v}_x &= -m\dot{\psi}v_y + \left(F_{xfl} + F_{xfr}\right)\cos\delta + F_{xrl} + F_{xrr} - \left(F_{yfl} + F_{yfr}\right)\sin\delta \\ m\dot{v}_y &= -m\dot{\psi}v_x + \left(F_{xfl} + F_{xfr}\right)\sin\delta + F_{yrl} + F_{yrr} + \left(F_{yfl} + F_{yfr}\right)\cos\delta \\ I_z\ddot{\psi} &= l_f\left(F_{xfl} + F_{xfr}\right)\sin\delta + l_f\left(F_{yfl} + F_{yfr}\right)\cos\delta - l_r\left(F_{yrl} + F_{yrr}\right) \\ &\quad + \frac{l_w}{2}\left(\left(F_{xfr} - F_{xfl}\right)\cos\delta + \left(F_{xrr} - F_{xrl}\right) + \left(F_{yfl} - F_{yfr}\right)\sin\delta\right) \end{aligned} \tag{1}$$

where δ represents the steering angle.

The front left, front right, rear left, and rear right tyre longitudinal tyre forces are F_{xfl}, F_{xfr}, F_{xrl}, and F_{xrr}, respectively. Similarly, the lateral forces may be stated as F_{yfl}, F_{yfr}, F_{yrl}, and F_{yrr}. The distances between the centre of gravity and the front and rear wheels, as well as between the left and right wheels, are denoted by the terms l_f, l_r, and l_w.

2.2 Wheel and tyre dynamics

The tyre/road interaction forces and moments for the wheels are required for the vehicle simulation. A general analytical tyre model (Dugoff et al., 1969) has been updated for combined wheel slip (Gunta and Sankar, 1980). The longitudinal wheel slip ratio, s_{xi}, becomes

$$s_{xi} = \begin{cases} \dfrac{r_{eff}\omega_{wi} - v_x}{v_x}, \ \mathrm{v}_x < r_{ref}\omega_{wi}; \text{ braking} \\ \dfrac{r_{eff}\omega_{wi} - v_x}{r_{eff}\omega_{wi}}, \ \mathrm{v}_x > r_{ref}\omega_{wi}; \text{ traction} \end{cases} \tag{2}$$

where the i subscript represents fl, fr, rl, rr. The term ω_{wi} denotes the ith wheels' rotational speed.

The front and rear tyre sideslip angles, α_i, become

$$\alpha_{fl} = \alpha_{fr} = \delta - \left(\frac{v_y + l_f\dot{\psi}}{v_x}\right), \ \alpha_{rl} = \alpha_{rr} = -\left(\frac{v_y - l_r\dot{\psi}}{v_x}\right) \tag{3}$$

The longitudinal and lateral tyre force, F_{xi} and F_{yi}, can be expressed as

$$F_{xi} = C_{\sigma i}\left(\frac{s_{xi}}{1+s_{xi}}\right)f\left(\lambda_i\right), \ F_{yi} = C_{\alpha i}\left(\frac{\tan\alpha_i}{1+s_{xi}}\right)f\left(\lambda_i\right) \tag{4}$$

where $C_{\alpha i}$ and $C_{\sigma i}$ are the cornering and longitudinal tyre stiffness. Using the wheel slip ratio, s_{xi}, and tyre sideslip angle, α_i, from equations (2) and (3), the variable λ_i and the function $f\left(\lambda_i\right)$ are given by

$$\lambda_i = \frac{\mu F_{zi}\left(1+s_{xi}\right)}{2\sqrt{\left(C_{\sigma i}s_{xi}\right)^2+\left(C_{\alpha i}\tan\alpha_i\right)^2}},\ f\left(\lambda_i\right)=\begin{cases}\left(2-\lambda_i\right)\lambda_i; & \lambda_i<1\\ 1; & \lambda_i\geq 1\end{cases} \tag{5}$$

The term F_{zi} represents the vertical force on the *i*th tyre while the symbol μ denotes the tyre-road friction coefficient.

The governing equation for the rotational wheel speed, ω_{wi}, may be expressed as

$$I_w\dot{\omega}_{wi} = T_{di} - T_{bi} - r_{eff}F_{xi},\ \left(i = fl, fr, rl, rr\right) \tag{6}$$

where I_w is the wheel inertia, and r_{eff} is the effective tyre radius. The drive and braking torque are denoted as T_{di} and T_{bi}.

2.3 Steering system dynamics

In a conventional steering scheme, a rack-and-pinion is generally linked to a steering wheel in a mechanical system. The steering wheel is replaced with a mobile device that is physically detached from the front wheels in a portable HMI guided system with steer-by-wire configuration. To actuate the front wheels, the driver's steering signals are sent electronically to an electric motor. Because the portable HMI uses drive-by-wire setting, an analytical model of the steering subsystem should be developed (Mills and Wagner, 2003).

Unlike traditional rack and pinion steering systems, the steer-by-wire system's directional control unit substitutes the steering column with a portable HMI and a high torque servomotor. The electric motor angular acceleration, $\ddot{\theta}_M$, differential equation becomes

$$\ddot{\theta}_M = \frac{1}{I_M}\left[-b_M\dot{\theta}_M - k_S\left(\theta_M - \frac{y_R}{r_P}\right) + T_M\right] \tag{7}$$

where I_M denotes the electric motor moment of inertia, b_M represents the motor damping coefficient, k_S is the lumped stiffness of motor shaft and the torque sensor inserted between the rack and the motor, and r_P is the pinion gear radius. The torque produced by the DC servomotor may be stated as $T_M = k_t i_a$ where the armature current, i_a, becomes

$$\frac{di_a}{dt} = \frac{1}{L}\left(-Ri_a - k_M\dot{\theta}_M + V\right) \tag{8}$$

In this expression, L denotes the motor electrical inductance, R represents the motor electrical resistance, and k_M is the motor electromotive force (e.m.f.) constant. The supply voltage, V, for this motor can be written as

$$V = \begin{cases} v_{\lim}, & \theta_{pH} > \varepsilon \\ k\theta_{pH}, & -\varepsilon < \theta_{pH} < \varepsilon \\ -v_{\lim}, & \theta_{pH} < -\varepsilon \end{cases} \tag{9}$$

where $v_{\lim} = 12V$ is the supply voltage saturation level, and $\varepsilon = 90°$ is the saturation limit for portable HMI steering angle θ_{pH}. The term θ_{pH} denotes the portable HMI steering angle and is given by

$$\theta_{pH} = K_{SR}\delta \tag{10}$$

where K_{SR} is the steering ratio between the turn of the portable HMI, θ_{pH}, and the turn of the front wheels, δ.

The rack displacement, y_R, may be expressed in differential equation form as

$$\ddot{y}_R = \frac{1}{m_R}\left[-2k_L\left(y_R - r_L\delta\right) - k_S\left(y_R - r_P\theta_M\right)\right] \tag{11}$$

where m_R is the rack-piston lumped mass, k_L denotes steering linkage stiffness, and r_L represents the kingpin axis offset at applied force.

The front wheel steering angle differential equation becomes

$$\ddot{\delta} = \frac{1}{I_w}\left[-k_L\left(\delta - \frac{y_R}{r_L}\right) - b_L\dot{\delta} - T_R\right] \tag{12}$$

where b_L is the front wheel assembly damping coefficient, and T_R is the aligning torque at the road-tyre interface.

3 Cellphone-inspired human machine interface

The motion-sensing 3-axis accelerometer is included in the simulated cellphone driving device (refer to Figure 3). Each of the device's three rotation axes is limited to $\pm 90°$. For this study, only the pitch and roll degrees-of-freedom for the portable device are used to control longitudinal and lateral vehicle motion. Communication between the portable controller and the vehicle computer is handled via a USB interface. An interface module obtains the raw acceleration data and converts it to roll and pitch signals which serve as the commanded steering angle and throttle-brake signal to operate specific actuators. The mapping of the pitch and roll orientation angles, θ_P, and θ_R (Wang et al., 2019a) from the driving interface actions are given by

$$\theta_{pH} = sat\left(\zeta/\theta_P\right)k_{in}\left|\theta_P\right| \tag{13}$$

$$T_{bi} = sat\left(\zeta/\theta_R\right)k_B\left|\theta_R\right|;\ \text{for}\ \theta_R \le 0 \tag{14}$$

$$T_{di} = sat\left(\zeta/\theta_R\right)k_D\left|\theta_R\right|;\ \text{for}\ \theta_R > 0 \tag{15}$$

where θ_{pH} is the mapped steering angle of the portable HMI and $\zeta = 90°$ is the saturation limit for raw pitch and roll angles data θ_P and θ_R. The saturation function $sat\left(\zeta/\theta_P\right)$ is given by

$$sat\left(\zeta/\theta_P\right) = \begin{cases} \zeta/\theta_P, & \left|\theta_P\right| \ge \zeta \\ \operatorname{sgn}\left(\zeta/\theta_P\right), & \left|\theta_P\right| < \zeta \end{cases} \tag{16}$$

The gain k_{in} correspond to the mobile interface steering angle and the terms k_B and k_D represents the brake and drive torque gains.

Figure 3 Handheld portable vehicle control device with longitudinal control features and integrated sensors (see online version for colours)

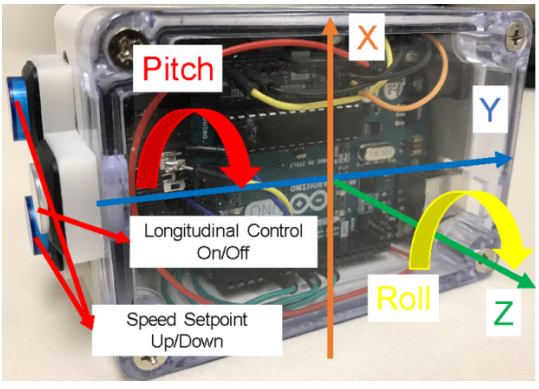

The portable driving HMI also incorporate longitudinal control (which is characterised in Section 4.1) to accurately maintain a speed set by the driver without any outside intervention. Isolating the throttle control from the steering input, the longitudinal control eliminates the user's distraction from lateral accelerations experienced while navigating a turn along with vertical and roll inputs from road disturbances. Side buttons on the device control the cruise feature with tap up/tap down functionality. As offered in passenger vehicles, the cruise controller interface allows speed setting and accelerate/decelerate using the three buttons. Table 1 summarises the steering properties of the traditional driving system, portable HMI, and steering subsystem (including tyres, wheels, DC motor, and steering linkages) in detail. The steering bandwidth is determined to inspect the maximum speed that the portable HMI, steering wheel, and front wheel assembly can be rotated during vehicle directional control.

Table 1 Comparison of steering system elements — steering wheel, portable HMI, and electric motor rack and pinion subsystem

	Steering wheel	*Portable HMI*	*Steering subsystem*
Inertia	*Medium*	*Low*	*High*
Degrees of rotation (°)	±270	±90	±30
Bandwidth (Hz)	$0.55 \leq BW \leq 1.20$	$0.42 \leq BW \leq 2.50$	$0.65 \leq BW \leq 1.16$

4 Control strategies for portable HMI

4.1 Longitudinal control design (cruise control)

Accurate throttle and brake control play an essential role to ensure that the automatic vehicle driving system achieves the desired longitudinal dynamic performance. To allow a portable HMI driven vehicle operating at a desired velocity setpoint,an optimal preview control which serves as a longitudinal speed-tracking controller based on reference and

feedback velocities is introduced. The technique was first proposed by MacAdam in (MacAdam, 1980) for synthesising closed-loop control of dynamic systems during tracking of previewed inputs is presented and was used to represents driver steering control behaviour during path-following and obstacle avoidance manoeuvres in MacAdam (1981). The proposed control strategy is governed by the properties of the controlled vehicle longitudinal system and is obtained by elimination of the previewed velocity error at a single point ahead in time.

4.1.1 Vehicle longitudinal dynamics

The longitudinal control aim is to minimise the vehicle longitudinal velocity concerning a given reference velocity. To implement the optimal preview control to the longitudinal vehicle dynamics, the vehicle longitudinal dynamics can be represented as

$$m\dot{v}_x = F_x - F_{aero} - F_{Rx} - mg\sin\theta \tag{17}$$

where $F_x = K_{pt}u$ is the total longitudinal tyre force, F_{aero} is the aerodynamics resistance force, F_{Rx} is the total rolling resistance force, and θ is the road inclination angle. The term K_{pt} is the effective vehicle total tractive force and u is the commanded throttle/brakecontrol signal.

The total rolling, driveline, and aerodynamic resistance $F_r = F_{aero} + F_{Rx}$ can be modelled as

$$F_r = \tanh\left(v_x\right)\left(\frac{a_r}{v_x} + c_r v_x\right) + b_r \tag{18}$$

where a_r is the rolling resistance coefficient, b_r is the driveline resistance coefficient, and c_r is the aerodynamic drag coefficient.

The state space model can be written as

$$\begin{cases} \dot{z} = Az + B\overline{u}, \overline{u} = u - \left(m/K_{pt}\right)g\sin\theta \\ y = Cz \end{cases} \tag{19}$$

Define the longitudinal position, x, and longitudinal velocity, v_x,so that the model states, z, can be expressed as

$$z = \begin{bmatrix} x \\ v_x \end{bmatrix}, A = \begin{bmatrix} 0 & 1 \\ 0 & F_r/m \end{bmatrix}, B = \begin{bmatrix} 0 \\ K_{pt}/m \end{bmatrix}, C = \begin{bmatrix} 0 & 1 \end{bmatrix} \tag{20}$$

4.1.2 Optimal preview control design

The optimal preview control is implemented to find the optimal control, $u^0(t)$, which minimises a local performance index (MacAdam, 1988)

$$J = \frac{1}{T}\int_t^{t+T}\left[v_{xref}(\eta) - y(\eta)\right]^2 d\eta \tag{21}$$

over the current preview interval $(t,t+T)$ where v_{xref} is the previewed velocity reference input. The previewed output, $y(t+T)$, is related to the current state, $z(t)$, and fixed control, $u(t)$, over the previewed interval $(t,t+T)$, by

$$y(t+T)=b^{*}z(t)+a^{*}u(t) \tag{22}$$

where a^{*} and b^{*} are the driver prediction scalar and vector gain, respectively, and can be found as

$$a^{*}=TC\left[I+\sum_{n=1}^{\infty}A^{n}T^{n}\Big/(n+1)!\right]B \tag{23}$$

$$b^{*}=C\left[I+\sum_{n=1}^{\infty}A^{n}T^{n}\Big/n!\right] \tag{24}$$

The term T is the preview time window, I is the identity matrix, and n is the number of states. Thus, the necessary condition that the derivative of J with respect to the control variable, u, be zero, offer the optimal control, u^{0}, as

$$u^{0}(t)=u(t)+\frac{e(t+T)}{a^{*}} \tag{25}$$

where $e(t+T)=v_{xref}(t+T)-y(t+T)$ is the previewed velocity error, which is being minimised in the original performance index in (21).

In order to account for the known neuromuscular delay of the driver, the resulting optimal control, $u^{0}(t)$, is assumed to be delayed an amount τ seconds. Thus, the commanded throttle/brake control input, $u(t)$, becomes (MacAdam, 1981)

$$u(t)=u^{0}(t)e^{-s\tau} \tag{26}$$

where $e^{-s\tau}$ is the driver transport time delay, and $u^{0}(t)$ is given in (25).

4.2 Lateral control design (lane keeping control)

A variable steering ratio control strategy will be proposed that provides lateral compensation to the driver and assists with lane keeping (Shimizu et al., 1999; Heathershaw, 2000; Nozaki et al., 2012). The steering ratio reflects the ratio between the portable HMI steering angle θ_{pH} the front wheel steering angle δ. The vehicle steering lightness may be directly tuned given the absence of a mechanical connection in the steer-by-wire system. For instance, low and high-speed steering sensitivity can be adjusted to enhance the vehicle overall handling performance. The steering system lateral controller encompasses feedforward and feedback components. The feedforward element considers human driving behaviour while the feedback action corrects for vehicle lateral placement in the roadway lane. Both control actions are summed to determine the steering ratio based on vehicle speed and position, commanded steering angle, and lane position desires. A high-level block diagram is presented in Figure 4. The steering ratio, $K_{SR}=K_{FF}+K_{FB}$, represents the control input of the system. This input is a combination of adaptive feedback control input, K_{FB}, and steering ratio feedforward control input, K_{FF}.

Figure 4 Lateral control design featuring feedforward and feedback actions embedded in the portable HMI

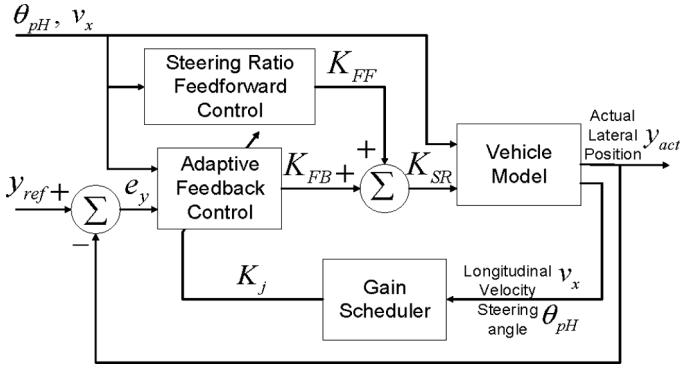

4.2.1 Adaptive feedback control

The main task of the lateral control is to adjust the steering angle such that the deviation between the desired and actual vehicle speeds is compensated. Unlike the steering wheel which can regulate its wheel steering angle through force feedback to the driver, the emulated cellphone driving device can change the steered wheel direction by adjusting the steering ratio which in turn modifies the steering angle. A gain-scheduling PID controller is developed as the feedback control for the portable HMI-steered vehicle to accomplish this task. The gain scheduling technique, an adaptive control method, is based on the adjustment of controller parameters in response to the vehicle's longitudinal speed and steering angle variations.

The steering ratio feedback output, $K_{FB}(t)$, of the gain-scheduling classical controller is given by

$$K_{FB}(t) = K_1(t)e_y(t) + K_2(t)\int e_y(t) + K_3\dot{e}_y(t) \tag{27}$$

where $e_y(t) = y_{act} - y_{ref}$ denotes the vehicle lateral error which is the orthogonal distance from the centre of gravity (CG) of the vehicle to the desired lane centre. The proportional, $K_1(t)$, integral, $K_2(t)$, and derivative, $K_3(t)$, gains of the gain scheduling controller have been determined to be time-varying parameters as follows

$$K_j = \sigma_j\left[\tanh\left(\rho_j k_s(t) - \eta_j\right) + \xi_j\right],\ j = 1,2,3 \tag{28}$$

where ρ is the sigmoid logistic growth rate, and the j subscript represents each time-varying gain in the steering ratio output.

The speed sensitive steer ratio, $k_s(t)$, is a function of portable HMI steering angle, $\theta_{pH}(t)$, and vehicle longitudinal velocity, $v_x(t)$, so that

$$k_s(t) = \frac{\theta_{pH}(t)}{v_x(t)} \tag{29}$$

The terms $\sigma_j = \frac{K_{jmax} - K_{jmin}}{2}$, $\eta_j = \frac{K_{jmax} + K_{jmin}}{2}$, and $\xi_j = \eta_j / \sigma_j$ are positive constants. The parameters K_{jmax}, and K_{jmin} are the upper and lower thresholds of the proportional, integral, and derivative gains. Note that by defining $k_s(t)$ directly proportional to the mobile interface steering angle θ_{pH} and inversely proportional to the vehicle longitudinal velocity $v_x(t)$, the gain scheduler can adjust the gain to adapt to the variations of driver steering behaviour and current vehicle state.

4.2.2 Steering ratio feedforward control

A feedforward steering ratio which varies according to the vehicle longitudinal speed as a fundamental characteristic is first considered. Then, compensation varying according to the portable HMI steering angle is incorporated in the feedforward control to attain a desirable steering ratio level (Wu et al., 2018).

The adaptive steering ratio feedforward control features a standard steering ratio during medium speed driving. The steering sensitivity declines as the vehicle speed increases and vice versa while the vehicle is deaccelerating. Such design guarantees a steering sensitivity level to ensure turning flexibility during low-speed driving (e.g., parking). Also, at high road speeds, a much lower road wheel steering angle input is required than at low speeds. Thus, a limited steering sensitivity is desired to provide steering stability during highway driving. To satisfy those design objectives in different speed conditions and to secure a smooth transition between each speed range, a logistic function with an increasing value of the steering ratio growth factor up to a desired steering stability level has been implemented in this study.

The steering ratio, K_v, which is shown in Figure 5(a) is computed as a logistic function of the vehicle longitudinal velocity, v_x, as

$$K_v = \frac{a + de^{-b(v_x - c)}}{1 + e^{-b(v_x - c)}} \tag{30}$$

where a and d are the maximum and minimum steering ratio, b is the curve logistic growth rate, and c is the vehicle speed of the sigmoid midpoint.

The steering ratio feedforward control also features a decelerated gear ratio near the straight-ahead position with the steering ratio quickening as the portable HMI steering angle increased further. On the road, this translates into smooth, confidence building lane changes and increased manoeuvreability when parking. On the other hand, such a design reduces steering sensitivity and enhances lateral stability during straight road driving. To accomplish such steering ratio changes concerning the portable HMI steering angle, a corner correction factor has been introduced. The corner correction factor, F_C, shown as Figure 5(b), is defined as a function of the portable HMI steering angle, θ_{pH}, using the Gaussian distribution or

$$F_C = h_1 e^{-\left(\frac{\theta_{pH} + p}{s}\right)^2} + h_2 e^{-\left(\frac{\theta_{pH} - q}{w}\right)^2} \tag{31}$$

where e is the natural logarithm base, and the terms h_1, h_2, p, s, w, and q are constants.

To obtain the best estimate of the feedforward control for the adaptive controller to account for the variation in longitudinal vehicle velocity and portable HMI steering angle, the feedforward steering ratio (displayed in Figure 5(c)) that considers human behaviour may be added to the control input

$$K_{FF} = F_C K_v \tag{32}$$

Figure 5 Variable steering ratio feedforward control: (a) Steering ratio of full-speed section varies with speed, (b) corner correction factor change with the portable HMI steer angle, and (c) the corrected steering ratio with the vehicle speed and mobile control interface angle changes (see online version for colours)

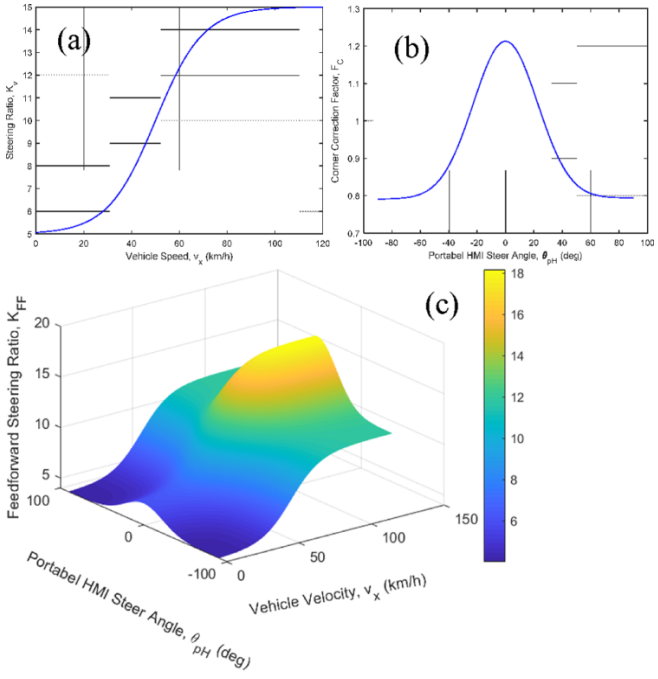

4.3 State flow controller (adaptive cruise control)

State flow control is a powerful logical strategy that utilises state machines and flow charts to model reactive systems and control complex nonlinear systems (Freeman et al., 2015). A state flow controller observes certain system states and discretely switches between pre-programmed control outputs. In this study, the state flow controller applies differential braking to help control the vehicle's longitudinal dynamics. The state transition logic expressions also incorporated driver operating parameters to reflect real-time driver intentions. The inclusion of driver prediction is indispensable for the successful development of an intelligent driver assistance systems.

To develop the driver intention algorithm for portable HMI steering, a set of steering and vehicle system parameters were selected (δ, $\dot{\delta}$, v_x, $\dot{v}_y$, $\dot{\psi}$). In other words, the requested front wheel steering angle, front wheel steering angle speed, vehicle speed, vehicle lateral acceleration, and vehicle yaw rate. Collectively, this information serves as a significant reflection of the driver's intention. Steering angle–zero to small steering

angle typically indicates a pursue of lane keeping while large steering angle deflection marks the cornering or obstacle avoidance intent from the driver. Steering angle speed – high steering angle speed suggests that an extreme manoeuvre is ongoing while small steering angle speed hints the driver is performing a low-speed cornering or switchback. Yaw rates and lateral acceleration – large values result from controlled steering manoeuvres such as turning, which signify the need for increased cornering ability. Small yaw rates and lateral acceleration imply a lack of need for cornering capability and occur during lane keeping or obstacle avoidance.

Based on these discussions above and experimental results completed by Wang et al. (2019a), three firing conditions for select driver intention states derived from the iterative experimental process are displayed in Figure 6(a).

A state flow braking controller, based on driver intention prediction, was designed to help reduce vehicle speed during turning manoeuvres and to maintain stability. The state flow braking controller coordinated with the other vehicle controllers by monitoring vehicle parameters and adjusting the brake torque, $T_{bi}\left(i=1,2,3,4\right)$, accordingly. These individual wheel brake torques were constrained conforming to physical limitations appropriate for each individual system. Additionally, the firing condition for different driver intention in Figure 6(b) serves as a transition condition that enables switching between different driving states while travelling various roadways. This strategy was implemented to help reduce controller complexity and mitigate the potential for instability at high speeds and large steering angles (Freeman et al., 2015).

The state flow braking controller consisted of three states, i.e., $S_{brake}=\left\{\text{Zero},\text{Obstacle},\text{Cornering}\right\}$, with the decision-making framework described below and shown in Figure 6(b) as a finite state machine (FSM).

Zero state: This state is the most commonly called state for portable HMI driving. In this state, the vehicle follows the planned path at a set speed, assisted by the optimal longitudinal controller and adaptive lateral controller. During regular vehicle operation, the braking controller operates in the zero state or OFF state, where no braking commands are implemented by the controller, i.e., $T_{bi}=0\,\text{N}\cdot\text{m}$. The braking controller remains in the Zero state until obstacle avoidance or turning event is detected, after which it transitions to either the Obstacle or Cornering state depending on steering and vehicle system parameters. The braking controller only returns to the Zero state if all four conditions in Condition A are met.

Obstacle state: In sudden obstacle avoidance cases, Obstacle state is invoked, and the driver will initiate a double lane change manoeuvre, during which the vehicle may travel on the roadway at high steering angle speed. In this case, small yaw rates and lateral accelerations imply a lack of need for cornering ability; thus, the longitudinal controller is temporarily disabled, and a large braking torque can be applied to help decrease the vehicle's longitudinal velocity.

Cornering state: The objective of the Cornering state is to distribute braking torque during braking whilst manoeuvring a curve. To accomplish this task, the previewed longitudinal controller velocity reference, v_{xref}, from equation (21) is decreased by 35%, and a reduced braking torque is applied in addition to the commanded brake control input, $u\left(t\right)$, from (26) to continue to provide some speed reduction while allowing more tyre traction for portable HMI steering manoeuvres.

Figure 6 (a) Firing conditions for three driver intention states: lane keeping, obstacle avoidance, and cornering/turning, and (b) logic flow for the SF braking control; controller state transitions based on comparison of vehicle states with firing condition (see online version for colours)

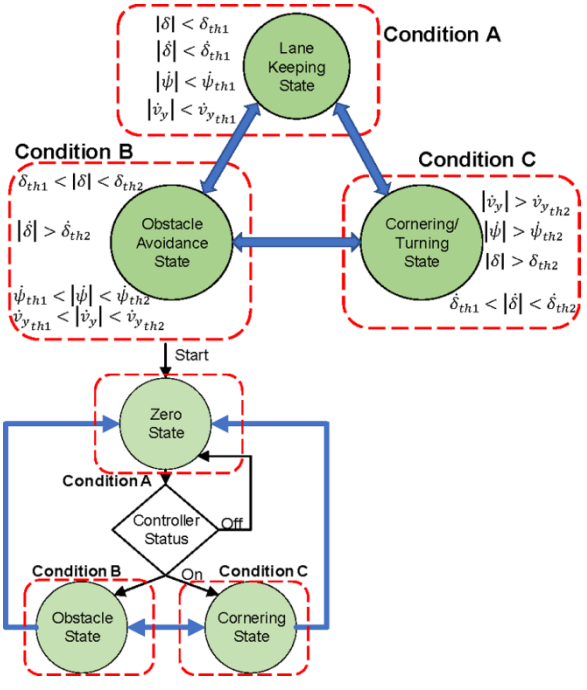

5 Experimental test bench

A fixed-based driving simulator was constructed to investigate the performance of operators driving utilising the portable HMI and traditional driving system. The simulator comprised the two driving interfaces (traditional driving system and portable HMI), a high-resolution image projector, and a Honda CR-V vehicle bench (see Figure 2). A total of $N = 30$ subjects participated ranging testing ages 18 to 31 with 22 males and eight females. The age demographic concentration matches the location of the university campus. The average number of years spent behind the wheel was 3.6. Ten of the participants admitted to playing cellphone racing games. Only one person responded yes when asked if they have driven a semi-autonomous vehicle. The driving sequence was modified for each subject to adjust for learning that may occur as a result of repeated activity. The portable HMI and steering wheel were tested in a randomised order thanks to a Latin square design. The following protocol was followed by each test subject:

1 Fill out a demographic survey to determine where each subject fits into the broader population.

2 To familiarise themselves with the system, subject trained driving at the target speed for several minutes.

3 Perform a test and record the vehicle and driver's responses.

4 For the specific driving event, the individual was asked to complete a post-test questionnaire.

5 Repeat with a different driving device and/or driving environment.

The performance of five different driving devices and control strategies (refer to Table 2) was investigated. Intuitively, the traditional driving system, with which operators are more experienced, should outperform the portable HMI in straight road driving scenarios. The conventional steering system coupled with the steering wheel featured self-centering feedback that allows the automatic return to centre after a turning manoeuvre, guaranteeing a decent cornering ability. On the other hand, portable HMI steering requires less physical movement, resulting in a faster steering response (Wang et al., 2019a). During intense manoeuvres, the driver's faster response time can enhance vehicle action. (e.g., obstacle avoidance). Additional control strategies implemented on the portable HMI may better vehicle handling, cornering capabilities, and safety functions (e.g., lane keeping, cruise control, adaptive cruise control) due to increased sophistication.

Table 2 System driving configurations

	Driving device	*Basic speed & directional control*	*Advanced control**			*Complexity*
			LK	*CC*	*ACC*	
C1	Steering wheel, foot pedal	✓				Low
C2	Portable HMI	✓				
C3		✓	✓			
C4		✓	✓	✓		
C5		✓	✓	✓	✓	High

Two hypotheses for the driving configurations have been proposed based on these factors:

H1: The traditional driving system, C1, is more applicable to the straight road and moderate cornering scenarios while the portable HMI, C2, possesses superior city road and extreme manoeuvre handling capabilities.

H2: The portable HMIs with different feedback controller combinations, C3-C5, will progressively enhance the vehicle safety performance compared to C2 as the control strategy sophistication increases.

6 Case studies with test results

Case studies were conducted in two separate driving environments: obstacle avoidance and city roadway driving. The scenario is limited owing to a tradeoff between model sophistication and execution speed. The best performance is achieved when an operator completes a given task with the least amount of lateral and heading error and optimal handling (e.g., lateral acceleration, yaw rate, etc.). Table 3 summarises the vehicle and control model characteristics as well as the database.

6.1 Obstacle avoidance test

An obstacle avoidance, ISO 3888-2 (2011), was tested in the simulator to compare the evasive manoeuvre performance of the four driving configurations (refer to Figure 7(a)). Figure 7(b) shows the dimensions of the 61m track as well as the cone location. The participants were instructed to enter the ISO test track at a speed of 50 kph, then drive from the original lane to an adjacent lane, then back to the original lane without displacing the cones placed alongside the track. The goal of obstacle avoidance is to allow the vehicle to achieve a series of alternating high lateral accelerations that can be used to analyse the vehicle's lateral dynamics. The test findings of Driver #6, who drove with the portable HMI or the standard driving system and did not strike or bypass any cones, will be addressed.

Table 3 Summary of vehicle and control model parameters

Symbol	*Value*	*Units*	*Symbol*	*Value*	*Units*
a_r	200	N	K_{2max}	1.5	m^{-1}
b_r	2.5	$\mathrm{N \cdot s/m}$	K_{2min}	0	m^{-1}
b_L	900	$\mathrm{kg \cdot m/s}$	K_{3max}	3.4	s/m
b_M	1.432	$\mathrm{kg \cdot m/s}$	K_{3min}	1	s/m
c_r	0.5	$\mathrm{N \cdot s^2/m^2}$	k_S	33.9	Nm/rad
$C_{\alpha f}$	5.04×10^{-4}	N/rad	k_t	2.65×10^{-3}	$\mathrm{N \cdot m/A}$
$C_{\alpha r}$	3.36×10^{-4}	N/rad	l_a	2	m
$C_{\sigma i}$	1.42×10^{4}	N	l_b	3	m
g	9.80	$\mathrm{m/s^2}$	l_c	3	m
I_M	0.075	$\mathrm{kg \cdot m^2}$	l_f	1.18	m
I_w	2.7	$\mathrm{kg \cdot m^2}$	l_r	1.77	m
I_z	1.89×10^{-4}	$\mathrm{kg \cdot m^2}$	m	1500	kg
k	1.33×10^{-1}	V/deg	m_R	29.4	kg
k_L	48.8×10^{-3}	$\mathrm{N \cdot m}$	r_{eff}	0.41	m
k_M	1.05×10^{-3}	Vs/rad	r_L	0.118	m
K_{pt}	3000	N	r_P	7.37×10^{-3}	m
K_{1max}	10.6	m^{-1}	τ	0.1	s
K_{1min}	2.1	m^{-1}	μ	0.85	

Figure 7 Virtual driving environment for human subject testing – (a) driver perspective of the obstacle avoidance event, and (b) top view of ISO 3888-2 obstacle avoidance track layout. Driver #6 response – (c) desired and actual vehicle trajectories, (d) lateral error, (e) steering device steering angle, and (f) Lateral acceleration when driving through the obstacle avoidance track with initial speed of 50 kph under configurations C1–C5 (see online version for colours)

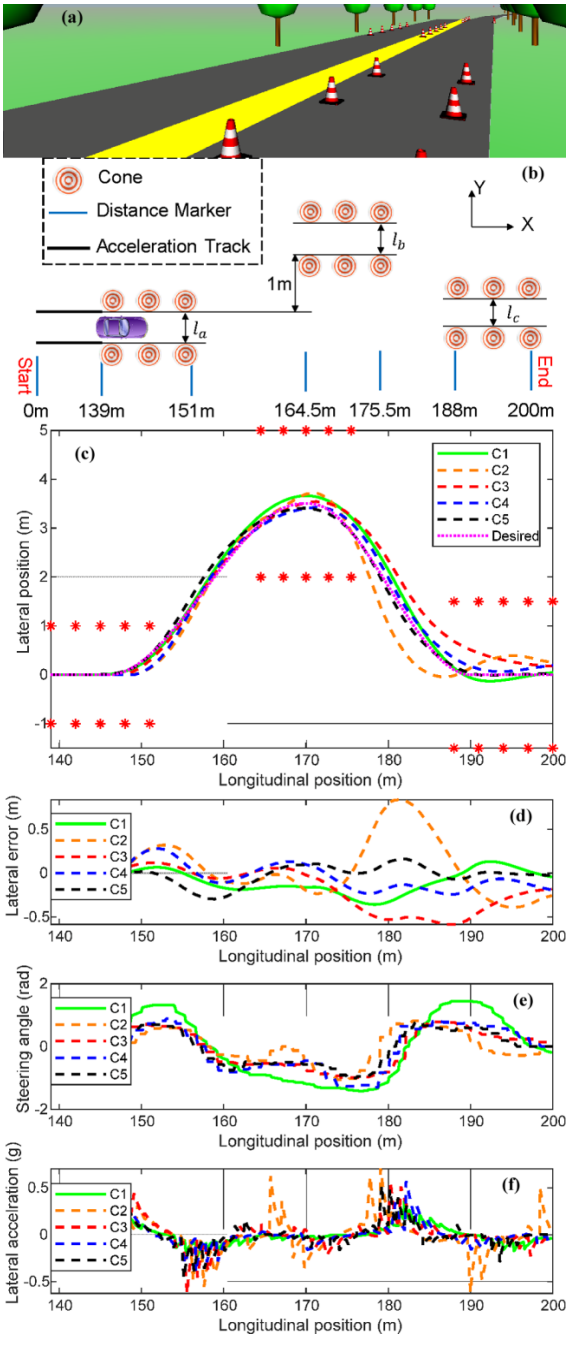

To demonstrate and compare the obstacle avoidance trajectory following capabilities for all five driving configurations, the vehicle paths and error with respect with the desired trajectory on the ISO track are plotted in Figures 7(c) and (d), respectively. Driver #6, who successfully completed the manoeuvre using both the steering wheel and portable HMI, travelled from 139m to 168m with minor lateral deviations with reference to the desired vehicle trajectory (Jalali et al., 2013). During the return sequence (168–200 m), each of the five variants had a noteworthy steering variance. Specifically, the desired path-following performance of the steering wheel, C1, is good and outperforms the configuration C2, which displays a winding driving pattern and the worst lateral stability with a maximum 0.84 m error. By adding the lane-keeping functionality to C2, C3 ameliorates the weaving behaviour and reduces the maximum lateral error by 30.4%. During the steering operation of C3, unintended portable HMI forward/backward rotations by the driver were observed, causing instantaneous speed instability and deteriorated performance. Consequently, the configuration C4, with the addition of the optimal preview longitudinal controller, decreases the lateral error by 58.3% through neutralising those accidental pitch rotations. Moreover, configuration C5, which provides automatic braking based on driver intent on top of C4, further enhanced the lateral performance of the portable HMI by lowering the maximum lateral error to 0.16 m. In extreme driving situations like obstacle avoidance, both braking and steering movement should be considered to safely and smoothly return the car to its original path. In general, as control sophistication increases (C2–C5), the lateral performance of the portable HMI improves.

The results for the driving devices steering angle are plotted in Figure 7(e). Noticeably, the driver used the steering wheel more forcefully to guide the car through the obstacle avoidance event, applying up to 1.45 rad (83°) at times. The tiny steering angles of portable HMI driving, on the other hand, required less effort, resulting in an easier and more comfortable steering experience. In addition, the steering directional adjustment speed on the portable HMI was faster than the steering wheel. Such agile steering rotation allows the driver to accomplish the aggressive manoeuvre quicker with the portable HMI, which in turn, ensures driver safety. The lateral acceleration variation vs. the longitudinal distance is shown in Figure 7(f). When steering with the portable HMI configurations, C2–C5, the lateral accelerations are generally larger than those steering with the traditional driving system, C1. The maximum lateral acceleration the driver experienced steering with configuration C2 reaches up to 0.62 g, which leads to severe motion sickness, considering the lateral acceleration limit to assure driver comfort is 0.4g. Overall, the portable HMI with all three controllers involved, C5, offers the best lateral performance and unchallenging driving experience during the obstacle avoidance.

6.2 City road test

To evaluate the performance of the portable HMI in an urban traffic environment, a city roadway has been established as illustrated in Figure 8(a). The urban scenario, which involves turns, intersections, and traffic, was designed to invoke the awareness of driving in the downtown area of a populated city. The road in Figure 8(b) has a 200 m straight section to achieve a 30 kph initial speed (a standard city street speed limit). After that, the driver must make a 15 m right turn at an intersection and an expressway ramp. Each road feature includes a straight path section that evaluates the vehicle's traction and stability on the straight road following a turn and serves as a recovery zone for the driver before

the next turn manoeuvre. Two potholes with orange cone hazard markers are placed on the straight road and the ramp tracks. On the map, the total distance travelled by the driver along the road has been marked.

Figure 8 Virtual driving environment for human subject testing – (a) driver perspective of the city road driving event, and (b) top view of city road track with two orange cones for hazard marker and distance travelled marker. Driver #9 when driving through the city roadway right turn with the speed of 30kph under configurations C1–C5 – (c) Pothole event roadmap (dashed line represents lane markings and red circle denotes the orange cone), (d) heading error for right turn manoeuvre, and (e) lateral error during right turn manoeuvre with C2 saturating corresponding to run off road event (see online version for colours)

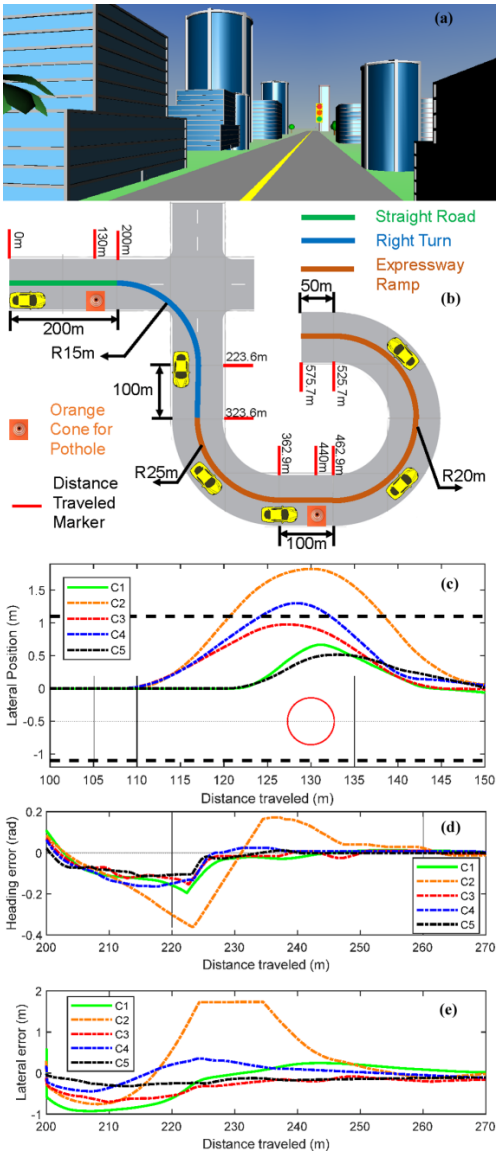

6.2.1 Straight road and ramp entry (distance 0–323.6 m)

During the acceleration phase, drivers will encounter a pothole to evaluate the manoeuvrability of the four driving configurations when handling this common obstruction. The drivers were asked to drive around the pothole, which is filled by an orange traffic cone. The vehicle trajectories of Driver #9for configurations C1–C5 are displayed in Figure 8(c). The traditional driving system, C1, accomplished the manoeuvre effectively thanks to the familiarity with the classical steering and braking. Noticeably, the vehicle operated using the portable HMIs that does not feature adaptive braking (e.g., C2, C4) travelled into the adjacent lane. In contrast, configuration C5 applied the brakes before and during the manoeuvre, ensuring minimal lateral deviations and lateral acceleration. This predictive brake system also boosted the driver handling confidence, as evidenced by the delayed pothole avoidance initiation.

Next, the driver encounters an intersection at which a 15 m radius right turn manoeuvre is performed. Given that the driver was negotiating the turn at 30 kph with a centrifugal acceleration of 0.472 g, such extreme cornering manoeuvres necessitated aggressive driving. Figures 8(d) and (e) show the vehicle's lateral and heading errors for Driver #9 to evaluate configurations C1–C5.Equipped with basic speed and directional control functionality, C2 demonstrates unsatisfactory performance with the largest maximum heading and lateral error. With the addition of the lane-keeping feature and variable steering ratio control, C3 not only ameliorated the understeer observed in C2 but also improved the yaw motion, decreasing the maximum heading error by 57.8%. The adoption of cruise control in C4 failed to improve the vehicle's lateral and yaw performance, as speeding occurred around the sharp turn that requires deceleration. The state flow controller applied brakes during the turn to reduce the speed, resulting in C5 exhibiting the lowest heading and lateral error. The traditional driving system, C1, with a maximum lateral error of 0.92 m, presented inferior lane-keeping ability compared to C2 during the turn (200–223.8 m). However, on the straight road following the turn (223.6–323.7 m), C1 lateral error is lower than C2, indicating that the steering wheel's self-centering feedback guarantees a remarkable realignment capability after a sharp turn.

6.2.2 Expressway ramp (distance 323.6–575.7 m)

The second road scenario features an expressway ramp with left curved roadways (323.6–575.7 m) for the vehicle to travel 270° to continue on the path. The change in ramp elevation is neglected for simplification purposes. The lateral errors of all 30 human subjects driving the expressway ramp are depicted in Figure 9(a). Isolating the extreme values and identifying the range of middle values, the boxplots identify symmetrical or skewed distributions among the lateral error data. Predictably, C1 outperformed C2 since the steering wheel with a larger rotational inertia can transfer more gradual steering commands to the vehicle which ensures a smoother cornering experience. The configuration C3 with lane-keeping feature and variable steering ratio control demonstrated a significant reduction in the lateral error of the portable HMI. The addition of longitudinal cruise control further reinforces the vehicle lateral stability as C4 displayed superior lane-keeping fulfilment compared to C3. By constantly adjusting the throttle to control the vehicle speed, C4 alleviated the lift-off oversteer which occurs when reducing the throttle mid-corner. The state flow controller in C5 applies an adaptive braking strategy during the cornering manoeuvres which impacted the lateral error due to

brake-induced oversteer. Collectively, although the portable HMI achieved inferior lateral performance on expressway ramp when compared to the traditional driving system, the addition of advanced control strategies enabled the mobile control interface to accomplish comparable lateral stability to the steering wheel.

The yaw rate, $\dot{\psi}$, vs. the steering device angle, θ_{pH}, was displayed in Figure 9(b) for all driving configurations on the city road to inspect the vehicle handling performance. A linear relationship is observed for both the portable HMIs and the steering wheel, suggesting good cornering performance. The portable HMI offers a substantially faster response and yaw rate than the steering wheel for on-centre steering. As a result, the car driven by the portable HMI is more responsive than the vehicle driven by the steering wheel. The portable HMI-driven vehicle's faster responsiveness and greater controllability in obstacle avoidance and turns were also explained by this correlation. Moreover, the steering device angle range of C5 is smaller than that of the other driving configurations (C1–C4). The adoption of the adaptive cruise control feature, C5, alleviated the physical steering efforts, which lighten the driver's burden during select manoeuvres.

Figure 9 (a) Statistical lateral error data for all $N = 30$ human subjects when driving through the expressway ramp, and the outliers are plotted individually using the red '+' symbol; the central mark on each box indicates the median, and the bottom and top edges of the box indicate the 25th and 75th percentiles, respectively. The whiskers correspond to the minimum and maximum of all the data, and (b) City road driving event yaw rate vs steering device angle (see online version for colours)

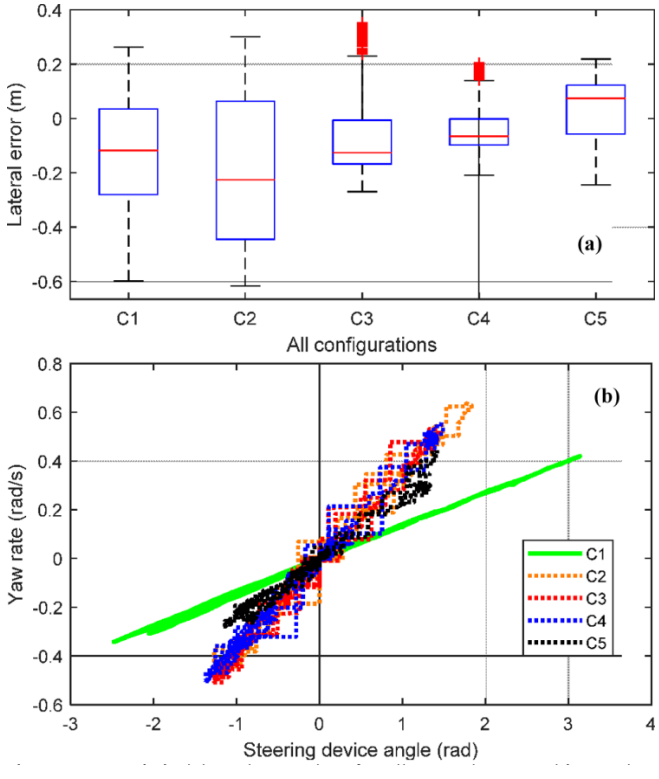

6.3 Questionnaire results

The subjective reactions of the human driver to the steering system feedback settings were evaluated through a questionnaire. As shown in Table 5, nine questions requested responses on a scale of 1 to 7. These questions explored three aspects: (i) The degree to which participants felt confident and in control of the driving system (Questions 1–4, symbol O1), (ii) The ease with which the driving system was perceived (Questions 5 and 6, symbol O2), and (iii) The vehicle's safety was understood (Questions 5 and 6, symbol O2) (Questions 7–9; symbol O3).

Figure 10 displays the normalised subjective reaction measures for the five driving configurations (C1–C5) and the driver observations (O1–O3). Because of their familiarity, participants gave the traditional driving method, C1, the highest ranking for the confidence and control measure, O1. Results also show that C5 received complimentary remarks from the drivers for its operational comfortableness and additional safety assurance during obstacle avoidance. One crucial observation found in the analysis of ease-of-use, O2, was that C4 and C5 were significantly preferred over C1 and C2. Such a novel pattern may be explained by the proposed advanced control systems and the intrinsic low weight of the portable HMI which required substantially less physical effort from the operator during both ordinary driving and evasive manoeuvring. Finally, it was observed that the safety, O3, rating was inversely correlated with lane deviations. Consequently, most operators rated high scores on C4 and C5 for the capability of driving the vehicle safest during moderate turns/cornering and sharp intersection turns, respectively.

Figure 10 Nine subjective measures based on driver's responses to the questionnaire in Table 5 were normalised to 10 for different driving configurations.O1 to O3 correspond to Table 5 and capture steering characteristic behind driver assessment (see online version for colours)

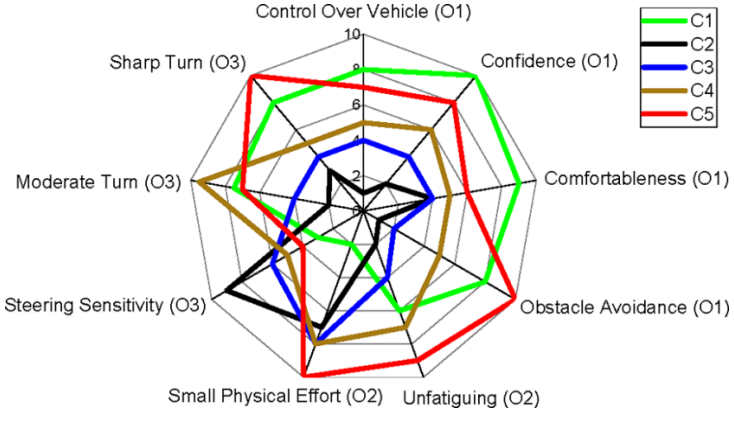

6.4 Summary of findings

To provide insight into the driver's understanding and execution of the obstacle avoidance and the city road scenarios for each driving configuration, the RMS yaw rate, $\dot{\psi}_{rms}$, lateral error, e_{lrms}, lateral acceleration, $\ddot{y}_{rms}$, and steering device angle, δ_{rms}, plus the average cones hit in each manoeuvre, N_{hit}, are listed in Table 4. Thirty human

subjects participated in the study. In terms of the lateral tracking performance, C5 not only prevailed over the other portable HMI configurations (C2–C4), but also demonstrated a 32.5% and a 55.8% lateral error decrease compared to the traditional driving system, C1, during obstacle avoidance and city road driving, respectively. On the other hand, C1 achieved the lowest lateral acceleration on both road scenarios, ensuring superior vehicle lateral stability and driver comfort. Also, the more substantial RMS steering device angle data obtained from C1, indicated that the drivers rotated the steering wheel more aggressively than the portable HMI. Lastly, C1 and C5 hit the least number of cones during the evasive manoeuvres in both obstacle avoidance and city road scenarios thanks to their lateral stability and superior handling performance.

Four significant findings may be inferred based on the evaluation factors and earlier discussions:

1 The traditional driving system, C1, performance dominates in straight and moderate road conditions. It outperforms the portable HMIin terms of on-centre handling linearity, lateral stability, and driver comfort.

2 The portable HMI, C2, proved to be in adequate in coping with both moderate driving and extreme manoeuvres. Specifically, not only does C2 exhibit the largest lateral deflection from the road centre, but it also yields a high yaw rate and lateral acceleration, which may lead to loss of traction and increased potential for rollover. The adoption of the lane-keeping feature improved the lateral instability, as evident by the reduction in the lateral error, lateral acceleration, and the number of cones hit with C3 compared to C2.

3 The integration of a longitudinal controller in the HMI device, C4, enhanced the vehicle's performance on the straight road and moderate cornering manoeuvre. However, drivers exhibited poor obstacle avoidance and sharp turn manoeuvres due to an inability to deaccelerate.

4 The introduction of driver intent-based state flow control in C5, which applies automatic predictive brakes, offered the best performance. In extreme manoeuvres such as sharp turn and obstacle avoidance, C5demonstrated the best lateral tracking capability and the least number of cones hit. The downside of C5 is that braking during a moderate turn can cause skidding or brake-induced oversteer.

The drivers manipulated the portable HMI with high frequency and small-amplitude actions during the obstacle avoidance scenario. In contrast, the steering wheel was operated with gradual, large-amplitude movements. It may be stated that quicker portable HMI steering direction adjustments may yield safety benefits in extreme manoeuvring situations like sharp turns and lane changes. However, the portable HMI does not offer much impedance to driver commands given the lightweight and compact nature of the enclosure. Consequently, steering commands may need to be further filtered to "smooth" the inputs to minimise hazardous driving.

Concerning the hypotheses H1 and H2, these experimental results show that H1 is partially invalid. Intuitively, configuration C2 possesses superior city road and extreme manoeuvre handling capabilities due to its faster steering response. In practice, however, most participants failed to adapt to the high steering sensitivity from C2, which leads to undesirable lateral performance. On the other hand, H2 cannot be fully settled. Even though C5 demonstrates its superiority in aggressive manoeuvres such as obstacle

avoidance, its reliability during moderate cornering remains questionable and deserves further investigation. More experiments and statistical analysis are required to demonstrate the efficacy of portable HMI under various road and speed circumstances.

Table 4 Summary of driver averaged performance of $N = 30$ subjects for different configurations and roadways (lower values in bold)

Test No.	*Road scenario*	*Design*	$e_{lrms}(m)$ $\times 10^{-1}$	$\ddot{y}_{rms}(m/s^2)$ $\times 10^{-1}$	$\delta_{rms}(rad)$ $\times 10^{-1}$	N_{hit} *cones hit*
1	Obstacle avoidance (50 kph)	C1	1.57	**3.74**	4.42	1.3
2		C2	3.17	7.88	4.27	4.4
3		C3	2.66	5.11	2.81	3.2
4		C4	1.47	4.39	**1.89**	1.1
6		C5	**1.06**	5.51	2.27	**0.6**
5	City road (30 kph)	C1	2.42	**1.14**	9.93	**0.03**
		C2	2.74	5.98	5.23	0.18
6		C3	2.30	5.55	4.86	0.11
7		C4	1.78	4.31	**4.40**	0.13
8		C5	**1.07**	3.33	5.50	0.06

7 Conclusion and future work

The worldwide growth in semi-autonomous ground vehicles necessitates alternative driving input devices adaptable to all drivers. In this study, a novel portable interface that combines steering, throttle, and braking functions in a holistic handheld device was designed, modelled, fabricated, and evaluated for ground vehicles. A series of vehicle dynamic models for the propulsion and directional control components, including the chassis, wheels and tyres, as well as steering system, have been derived. Three control strategies, including variable steering ratio control, optimal preview control, and state flow control, were developed and implemented on the portable HMI for lane-keeping, cruise control, and adaptive cruise control functionalities. Human test subjects operated the mobile control device in obstacle avoidance and city road conditions. The case studies revealed that the mobile driving interface, with the assistance of appropriate control strategies, could evenly match or outperform the traditional driving system in selected manoeuvres. Test results showed that the driver's experience can be enhanced up to 55.8% with the portable HMI when compared to the traditional steering wheel.

The experimental findings offer some intriguing opportunities for future research. First, the alternative HMI should be installed and field-tested in a drive-by-wire vehicle to validate the concept. Second, the biomechanics of this novel driving device should be examined to explore the side effects of long-term usage regarding wrist fatigue and injuries. Third, drive-by-wire failsafe measures and security protocol should be explored to ensure driver and occupant safety.

References

Andonian, B., Rauch, W. and Bhise, V. (2003) 'Driver steering performance using joystick vs. steering wheel controls', in', *SAE 2003 World Congress & Exhibition*, Detroit, MI, pp.2003-01–0118.

Attia, R., Orjuela, R. and Basset, M. (2014) 'Combined longitudinal and lateral control for automated vehicle guidance', *Vehicle System Dynamics*, Vol. 52, No. 2, pp.261–279.

Chebly, A., Talj, R. and Charara, A. (2017) 'Coupled longitudinal and lateral control for an autonomous vehicle dynamics modeled using a robotics formalism', *IFAC-PapersOnLine*, Vol. 50, No. 1, pp.12526–12532.

Dugoff, H., Fancher, P.S. and Segel, L. (1969) *Tire Performance Characteristics Affecting Vehicle Response to Steering and Braking Control Inputs*, Highway Safety Research Institute Institute of Science and Technology, The University of Michigan Ann Arbor, Michigan, p.109.

Elvin, D. and Gambrell, P. (2002) 'Adapting vehicles for the disabled driver', *International Body Engineering Conference & Exhibition and Automotive & Transportation Technology Congress*, New Orleans, LA, pp.2002-01–2082.

Fong, T.W., Conti, F., Grange, S. and Baur, C. (2001) 'Novel interfaces for remote driving: gesture, haptic, and PDA', in Choset, H.M., Gage, D.W. and Stein, M.R. (Eds.): *Intelligent Systems and Smart Manufacturing*, Boston, MA, pp.300–311.

Freeman, P., Jensen, M., Wagner, J. and Alexander, K. (2015) 'A comparison of multiple control strategies for vehicle run-off-road and return', *IEEE Transactions on Vehicular Technology*, Vol. 64, No. 3, pp.901–911.

Freeman, P., Wagner, J. and Alexander, K. (2016) 'Run-off-road and recovery–state estimation and vehicle control strategies', *Vehicle System Dynamics*, Vol. 54, No. 9, pp.1317–1343.

Gambrell, P. and Elvin, D. (2002) 'The application of new technologies in the motor car-positives and negatives for the disabled driver', *International Body Engineering Conference & Exhibition and Automotive & Transportation Technology Congress*, New Orleans, LA, pp.2002-01–2083.

Gil, J.J., Díaz, I., Ciáurriz, P. Echeverría, M. (2013) 'New driving control system with haptic feedback: design and preliminary validation tests', *Transportation Research Part C: Emerging Technologies*, Vol. 33, pp.22–36.

Gunta, R. and Sankar, S. (1980) 'A friction circle concept for Dugoff's tyre friction model', *International Journal of Vehicle Design*, Vol. 1, No. 4, pp.373–377.

Guo, J. (2016) 'Coordinated longitudinal and lateral control of autonomous electric vehicles in a platoon', *SAE-TONGJI 2016 Driving Technology of Intelligent Vehicle Symposium*, Shanghai, China, pp.2016-01–1875.

Guo, J., Hu, P. and Wang, R. (2016) 'Nonlinear coordinated steering and braking control of vision-based autonomous vehicles in emergency obstacle avoidance', *IEEE Transactions on Intelligent Transportation Systems*, Vol. 17, No. 11, pp.3230–3240.

Heathershaw, A. (2000) 'Optimizing variable ratio steering for improved on-centre sensitivity and cornering control', *SAE 2000 World Congress*, Detroit, MI, pp.2000-01–0821.

ISO 3888-2: 2011 (2011) International Organization for Standardization, Available at: http://www.iso.org/cms/render/live/en/sites/isoorg/contents/data/standard/05/72/57253.html (Accessed 31 July, 2019).

Jafari, N., Adams, K.D. and Tavakoli, M. (2016) 'Haptics to improve task performance in people with disabilities: a review of previous studies and a guide to future research with children with disabilities', *Journal of Rehabilitation and Assistive Technologies Engineering*, Vol. 3, p.205566831666814.

Jalali, K., Rahmani, M., Charkhgard, H. and Kasaiezadeh, A. (2013) 'Development of an advanced fuzzy active steering controller and a novel method to tune the fuzzy controller', *SAE International Journal of Passenger Cars – Electronic and Electrical Systems*, Vol. 6, No. 1, pp.241–254.

Katriniok, A., Lienkamp, M. and Winner (2013) 'Optimal vehicle dynamics control for combined longitudinal and lateral autonomous vehicle guidance', *2013 European Control Conference (ECC)*, *2013 European Control Conference (ECC)*, IEEE, Zurich, pp.974–979.

Kim, I-H., Lee, K. and Kim, H-K. (2017) 'Prediction of driver's intention of lane change by augmenting sensor information using machine learning techniques', *Sensors*, Vol. 17, No. 6, p.1350.

Kumar, P., He, Y. and Wu, Q.M.J. (2013) 'Learning-based approach for online lane change intention prediction', *2013 IEEE Intelligent Vehicles Symposium (IV)*. *2013 IEEE Intelligent Vehicles Symposium (IV)*, Gold Coast City, IEEE, Australia, pp.797–802.

Li, K., Zhang, H. and Wu, J. (2016) 'Lane changing intention recognition based on speech recognition models', *Transportation Research Part C: Emerging Technologies*, Vol. 69, pp.497–514.

MacAdam, C.C. (1980) 'An optimal preview control for linear systems', *Journal of Dynamic Systems, Measurement, and Control*, Vol. 102, No. 3, p.188.

MacAdam, C.C. (1981) 'Application of an optimal preview control for simulation of closed-loop automobile driving', *IEEE Transactions on Systems, Man, and Cybernetics*, Vol. 11, No. 6, pp.393–399.

MacAdam, C.C. (1988) *Development of Driver/Vehicle Steering Interaction Models for Dynamic Analysis*, UMTRI-88-53, University of Michigan Transportation Research Institute, Ann Arbor, MI.

Matsuura, Y., Kitazawa, S. and Hiraike, Y. (2004) 'A study of driver's maneuver characteristics using the joy-stick device', *SAE 2004 World Congress & Exhibition*, Detroit, Michigan, USA, pp.2004-01–0452.

Mills, V.D. and Wagner, J.R. (2003) 'Behavioural modelling and analysis of hybrid vehicle steering systems', *Proceedings of the Institution of Mechanical Engineers, Part D: Journal of Automobile Engineering*, Vol. 217, No. 5, pp.349–361.

Nahak, S. and Kota, N. (2013) 'Modeling and amp; simulation of joystick operated steering system', *8th SAEINDIA International Mobility Conference & Exposition and Commercial Vehicle Engineering Congress 2013 (SIMCOMVEC)*, Chennai, India, pp.2013-01–2865.

Nozaki, H., Mizuno, K. and Yoshino, T. (2012) 'Effect of rear-wheel active steering and variable steering wheel gear ratio on proportional derivative steering assistance', *SAE 2012 Commercial Vehicle Engineering Congress*, , Rosemont, Illinois, USA pp.2012-01–1936.

Polling, D., He, X. and Ji, Q (2005) 'Inferring the driver's lane change intention using context-based dynamic Bayesian networks', *2005 IEEE International Conference on Systems, Man and Cybernetics*. *2005 IEEE International Conference on Systems, Man and Cybernetics*, IEEE, Waikoloa, HI, USA, pp.853–858.

Shaw, G., Dalrymple, G. and Ragland, C. (1999) 'Reducing the risk of driver injury from common steering control devices in frontal collisions', in', *International Congress & Exposition*, Detroit, Michigan, USA, pp.1999-01–0759.

Shimizu, Y., Kawai, T. and Yuzuriha, J. (1999) 'Improvement in driver-vehicle system performance by varying steering gain with vehicle speed and steering angle: VGS (variable gear-ratio steering system)', *International Congress & Exposition*, pp.1999-01–0395.

Wang, C., Zhang, Y., Liao, K. and Wagner, J.R. (2019a) 'Use of cellphones as alternative driver inputs in passenger vehicles', *WCX SAE World Congress Experience*, , Detroit, Michigan, USA pp.2019-01–1239.

Wang, C., Wang, Y. and Wagner, J.R. (2018) 'Evaluation of alternative steering devices with adjustable haptic feedback for semi-autonomous and autonomous vehicles', *WCX World Congress Experience*, Detroit, Michigan, USA, pp.2018-01–0572.

Wang, C., Wang, Y. and Wagner, J.R. (2019b) 'Evaluation of a robust haptic interface for semi-autonomous vehicles', *SAE International Journal of Connected and Automated Vehicles*, Vol. 2, No. 2, pp.12-02-02–0007.

Wu, Y., Wang, L. and Li, F. (2018) 'Research on variable steering ratio control strategy of steer-by-Wire system', *Intelligent and Connected Vehicles Symposium*, pp.2018-01–1583.

Xu, L., Chen, H., Huang, J., Wu, J. and Zhang, Y. (2016) 'Integrated longitudinal and lateral control for Kuafu-II autonomous vehicle', *IEEE Transactions on Intelligent Transportation Systems*, Vol. 17, No. 7, pp.2032–2041.

Zheng, H., Ma, S. and Na, X. (2017) 'Design of a variable steering ratio for steer-by-wire vehicle with a joystick', *Advances in Mechanical Engineering*, Vol. 9, No. 11, p.168781401773075.

Appendix

A Subjective questionniare

Table 5 Subjective questionnaire for evaluations of four driving configurations

Question	*Category*
1. I had good control over the vehicle.	Confidence and control (O1)
2. I felt confident in my ability to drive the vehicle safely.	
3. I was comfortable driving this vehicle on the roadway.	
4. I felt that I could drive this vehicle safely if I had to perform an obstacle avoidance on the road.	
5. Driving this vehicle for a long distance would make me tired.	Ease-of-use (O2)
6. I had to apply a lot of physical effort to command the vehicle to go where I wanted.	
7. The steering was too sensitive on this vehicle.	Safety (O3)
8. I felt that I could drive this vehicle safely at moderate turns or cornering	
9. I felt that I could drive this vehicle safely at sharp turns.	